Spectrum Analyzer Based Phase Measurement for Near-Field EMI Scanning

Shubhankar Marathe, *Student Member, IEEE,* Zongyi Chen, Kaustav Ghosh, *Student Member, IEEE,* Hamed Kajbaf, *Senior Member, IEEE,* Stephan Frei, *Senior Member, IEEE,* Morten Sørensen, *Member, IEEE,* David Pommerenke, *Fellow, IEEE,* and Jin Min

***Abstract*—Often EMI scanning applications require phase and magnitude information for the creation of equivalent radiation models and far-field predictions. Magnitude information can be obtained using a spectrum analyzer, which is relatively inexpensive compared to phase resolving instruments such as vector network analyzers and oscilloscopes at tens of GHz. This work introduces and optimizes a cost-effective spectrum analyzer-based phase measurement method and compares the results to a vector network analyzer and oscilloscope based methods for EMI signal sources. The measured phase distribution obtained from the three different instruments is additionally compared with the simulated phase determined from full-wave simulation. The three measurement methods are compared based on the type of signal spectrum to be measured, such as single or multiple frequencies, signals requiring low resolution bandwidth measurements, or transient signal events. The spectrum analyzer-based phase measurement technique is designed to operate from 5 GHz to 12 GHz. However, the system frequency bandwidth is limited only by the frequency bandwidth of the individual RF components used in the spectrum analyzer measurement system.**

***Index Terms*—Electromagnetic interference (EMI), near-field measurements, oscilloscope, phase-resolved measurements, probes, spectrum analyzer (SA), vector network analyzer (VNA).**

II. Introduction

EMI scanning applications require the phase information of the near-field E- or H- field data along with the magnitude for creating equivalent radiation models and far-field prediction. These applications include emission source localization methods such as emission source microscopy (ESM) [1], building an equivalent Huygen's box model for the noise source analysis [2]-[6], and near-field to far-field transformation (NFFFT) [4]-[6].

Near-field data obtained from a scanning plane above the device under test (DUT) is measured by using E and H probes [7]-[9]. For precise positioning and spatial resolution of the near-field scanned data, a robot scanning system is used. The output of a probe is a voltage when placed in the near-field of a noise source. The corresponding field to the probe voltage output is determined by a probe factor calibration measurement in the frequency-domain or time-domain measurement methods [10]-[12]. The quality of the scanned data is typically determined by the probe sensitivity (narrowband or broadband), the probe's capability to suppress the unwanted components, and the spatial resolution of the data obtained over a scan plane.

In phase-resolved scanning, one near-field probe (main probe signal) is moved along the DUT scan area to measure the magnitude. To obtain a phase reference signal (reference probe signal), a second probe measures from a fixed location or the signal is conductively probed inside the DUT. Methods for performing phase measurements using an oscilloscope or the VNA as receivers have been reported in the literature [12], [13].

VNA in normal operation measures phase with respect to its internal RF source for S-parameter measurements. As illustrated in [13], the VNA is used in tuned receiver mode, where it measures the phase of the signal based on an external source reference. The challenges related to using this mode are the poor image and spurious rejection in many VNA models. This is especially a drawback if the DUT spectrum contains many noise sources and their related harmonics. On the other hand, the oscilloscope method performs a measurement in the time-domain, performs a fast fourier transform (FFT), and determines the phase difference by subtracting the phase value between the main probe signal and the reference probe signal. One advantage of this method is the ability to trigger on the time-domain signal of interest, whereas the cost and the availability of high-frequency bandwidth oscilloscopes (above 4 GHz) is a challenge.

The availability and lower costs of swept frequency spectrum analyzers (SA) for high frequency make them a suitable choice for near-field scanning. However, SAs can only resolve the magnitude of the signal. If both phase and magnitude of field data are desired, additional devices/components are needed to calculate phase from magnitude-based SA measurements [14]-[17].

In [14]-[15], the method uses a 0° hybrid coupler to obtain the summation of the main probe signal and the reference probe signal. It requires three measurements with different setup configurations to obtain the phase information at a single frequency of interest. Thus, this phase detection method was developed for a single frequency operation. The analysis presented in [14]-[15] showed that the SA method only works

Manuscript received December 28, 2018. This work was supported in part by the National Science Foundation under Grant IIP-1440110.

S. Marathe, K. Ghosh, M. Sørensen, and D. Pommerenke are with the EMC Laboratory, Missouri University of Science and Technology, Rolla, MO 65409 USA (e-mail: skmcr4@mst.edu; kgkb4@mst.edu; sorensenmo@mst.edu; davidjp@mst.edu).

Z. Chen was with the On-Board Systems Lab, TU Dortmund University, Dortmund 44227, Germany. She is now with HELLA GmbH & Co. KGaA, Lippstadt, 59552, Germany (email: zongyi.chen@tu-dortmund.de).

S. Frei is with the On-Board Systems Lab, TU Dortmund University, Dortmund 44227, Germany (email: stephan.frei@tu-dortmund.de).

H. Kajbaf, and J. Min are with the Amber Precision Instruments (API), San Jose, CA 95134, USA (email: hamed@amberpi.com; jinmin@amberpi.com).

if the magnitudes of the main probe signal and the reference probe signal are similar.

To overcome the magnitude differences between the two input signals, a variable attenuator is introduced in the reference probe signal path of the setup. The SA method is improved to perform a broadband measurement [16]-[17], which was one of the shortcomings of the hybrid coupler-based phase measurement using the SA mentioned in [14]-[15].

In this paper, the SA based measurement technique is further improved in its computation time, phase-resolving optimization algorithm, and the setup is completely automated, thus, requiring no user intervention during the measurements. The setup makes use of a switch to use different phase-shift cable lengths and make multiple measurements to obtain the correct phase based on magnitude only SA measurements. The magnitude and phase information of a DUT is obtained using the SA method and compared with the measurement results from the VNA and oscilloscope. In addition, the measured data is also compared with full-wave simulation data. Further, section IV discusses the relative advantages of each method and the performance for different measurement test scenarios.

III. Phase Measurement Methods

This section describes the SA, VNA, and the oscilloscope-based measurement methods.

A. Spectrum Analyzer-Based Method

In a near-field scanning measurement, the main probe signal is obtained from the DUT scan plane, and a reference signal from a fixed location on the DUT. These two signals can be considered as two input vectors $\vec{A}$ and $\vec{B}$, where A and B are the magnitude and $\emptyset_a$ and $\emptyset_b$ are the phase of the respective vectors. The summation of the two vectors can be denoted by

$$\vec{C} = \vec{A} + \vec{B} \tag{1}$$

$$\vec{A} = Ae^{i\phi_a}, \vec{B} = Be^{i\phi_b} \tag{2}$$

where the summation vectors $\vec{A}$ and $\vec{B}$, is given by the vector $\vec{C}$. The spectrum analyzer instrument measures the magnitude of a signal. Thus, it is capable to determine the magnitude C, which represents the summation of the vectors $\vec{A}$ and $\vec{B}$ given by

$$C = \sqrt{\vec{C}\cdot\vec{C}} = \sqrt{(\vec{A}+\vec{B})\cdot(\vec{A}+\vec{B})}$$
$$= \sqrt{A^2 + B^2 + 2AB\cos(\phi_b - \phi_a)} \tag{3}$$

If the magnitude of the two vectors $\vec{A}$ and $\vec{B}$ are known, and the magnitudes are not too different, then identifying the phase difference φ is partially possible. For instance, if the magnitude A and B are measured and the summation magnitude C is also measured using an SA, using (3) the phase difference φ can be calculated. However, in this analytical calculation the sign information of the phase φ is lost. Because, the arccosine function provides the phase angle information only between 0° to + 180°, but not the phase angle information between 0° to – 180° (where, – 180° < φ < + 180°). Thus, to determine the sign (positive or negative) information of the phase difference φ, additional measurements are required. The sign information can be calculated by introducing a known phase shift $\emptyset_4$ between the two input signals, and measuring the phase shifted summation signal. The phase difference between the two input vectors is φ'. Using the equations proposed by the authors in [14]-[15], the sign information can be determined using the summation of the two input vectors, and the phase shifted summation measurements. Here, the two input vectors are needed to be of similar magnitudes to obtain the correct phase difference between the two input vectors.

1) Qualitative description of the single and multi-frequency scanning: A DUT can have one or multiple noise frequencies. Near-field scanning can be performed over the DUT scan area for all the desired noise frequencies. For instance, for a single frequency scanning application, only three measurements are required. First, measure the reference magnitude. Second, measure the probe magnitude. Third, measure the summation of the reference and probe magnitude with and without the known phase shift on the reference signal. Here, before measuring the summation of the reference and the probe magnitudes, the two magnitudes need to be compared. If the probe magnitude is much weaker than the reference magnitude, then sufficient attenuation has to be introduced on the reference signal to obtain similar magnitudes and then obtain the summation.

However, in a broadband scanning scenario multiple frequencies are of interest. For example, phase information of signals from 5 GHz to 10 GHz is desired. The SA can be configured to measure a span of 5 GHz in the desired frequency range. In most real-world measurement scenarios, multiple frequencies of interest will not have the same magnitude at a given scan point. In addition, the signal magnitude for multiple frequencies will vary as a function of the distance from the noise source location. However, the summation of the signals will only reveal the phase if the magnitudes of the two siganls are not too different. Thus, in this multiple frequency scanning scenario, the measurement is performed with different attenuation levels at the same scan point. Then, during the post-processing, the reference and the probe signals at the suitable attenuation setting having similar magnitudes are used to determine the phase difference. The specific implementation details are further described in the subsection II.A.3.

2) SA-based measurement system hardware: Fig. 1 depicts the setup used for near-field scanning measurements. The spectrum analyzer [18] measures the magnitude. The controlling computer uses an automation script written in Matlab [19]. The computer communicates with the SA using an Ethernet/LAN port for trace data acquisition, and for providing the instrument settings. The USB DAQ card is used to send out analog and digital voltage signals to control the variable attenuator and the SP3T switches. The switches require a 28 V external power supply. The digital output of the USB DAQ card is applied to the relays inside the switch control board. The switch control board selects one transmission path at a time. Thus, selecting

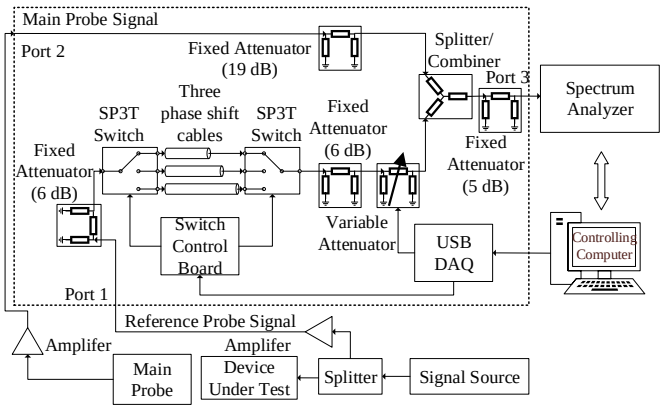

Fig. 1. SA measurement setup block diagram. The components in the dotted box frame represent the additional set of RF hardware components required to resolve phase using magnitude only measurements. The components below the dotted box frame represents the specific DUT setup used in this work.

between one out of the three phase-shift cables. The analog output of the USB DAQ card is applied to the voltage controlled (variable) attenuator. A wideband analog voltage controlled attenuator HMC712LP3C was used in this setup.

In the qualitative description depicted in Fig. 2, if the two signals are added in phase (0°), the maximum magnitude is obtained. Similarly, in the out of phase (180°) vector addition, a minimum value is obtained. Here, if the two signals are of similar magnitude, the difference between the maximum and the minimum is large. However, if the two input signals do not have similar magnitudes, then the difference between the maximum and minimum is small. Thus, if one vector has significantly larger magnitude than the other, it will dominate the vector summation and, hence, a small measurement uncertainty will introduce a large uncertainty in the phase difference estimation between the two vectors. In a practical broadband implementation, introducing a 180 ° phase shift between the two input signals is not possible for all frequencies of interest. Thus, a fixed value of phase-shift is introduced at a given frequency of interest by using RF components such as RF ICs, or coax cables. Therefore, in order to resolve the phase information between the two signals in a broadband measurement setup, the summation vector magnitude with and without the introduced phase-shift should have similar magnitudes.

Fixed value attenuators are used in this setup to improve the input match. Thus, the input reflections can be neglected. The splitter/combiner is used to add the signals from the reference probe signal path and the main probe signal path. A coaxial power splitter/combiner ZFRSC-123+ with a frequency

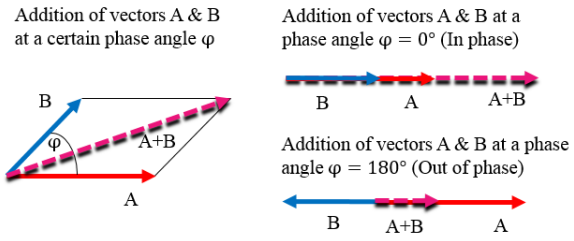

Fig. 2. Qualitative description of the vector addition of two input signals as a function of phase difference of 0°, 180°, and at an angle between 0° and 180°.

bandwidth up to 12 GHz was selected. Here, it is assumed that the reference probe signal selected for the measurement is one of the strong signals from the DUT. If the main probe signal power is within 30 dB (dynamic range of the variable attenuator) of the reference probe signal, the phase difference between the two signals can be resolved using the proposed setup. However, this 30 dB range can be further improved by using a wider-attenuation range variable attenuator.

The SA based measurement system hardware has multiple cables, splitters, switches, and the usage of a voltage controlled attenuator. The SA system S-parameters are measured to characterize the SA system in magnitude and phase. It is critical to use a dedicated stable voltage supply for the analog voltage controlled attenuator to maintain good attenuator repeatability in the setup. Variations in the supply voltage introduced undesired change in the variable attenuation value, thus, introducing errors in the phase estimation. In addition, the 3-port system S-parameters showed variations within +/- 0.5 dB during dismounting and mounting of the setup connections. The setup S-parameters are used to remove their magnitude and phase contribution from the measured DUT magnitude and DUT phase information.

3) Phase resolving methodology: Before initiating the scan, a signal should be determined from the DUT which can be used as the reference signal. It is assumed that this signal is from a fixed location on the DUT, and is stable throughout the desired scan time. Here, the selection of the reference probe signal from the DUT must include significant contributions from all the multiple freqeuncies of interest. In the automated setup as shown in Fig. 1, there are two paths (main probe signal path and the reference probe signal path) from the DUT which are added at the combiner and measured at the SA. The measured powers can be represented using the relation given by

$$P_{sum} = \frac{1}{2}\cdot\left(\left|b_{sum}\right|^2\right) = \frac{1}{2}\cdot\left(\left|S_{31}a_1 + S_{32}a_2\right|^2\right)$$
$$= \frac{1}{2}\cdot\begin{pmatrix}\left|S_{31}\right|^2\left|a_1\right|^2 + \left|S_{32}\right|^2\left|a_2\right|^2 + \\ 2\left|S_{31}\right|\left|a_1\right|\left|S_{32}\right|\left|a_2\right|\cos\left(\phi_1 - \phi_2 + \varphi\right)\end{pmatrix} \quad (4)$$

$$P_{sum\_c1} = \frac{1}{2}\cdot\left(\left|b_{sum\_c1}\right|^2\right) = \frac{1}{2}\cdot\left(\left|S_{31\_c1}a_1 + S_{32\_c1}a_2\right|^2\right)$$
$$= \frac{1}{2}\cdot\begin{pmatrix}\left|S_{31\_c1}\right|^2\left|a_1\right|^2 + \left|S_{32\_c1}\right|^2\left|a_2\right|^2 + \\ 2\left|S_{31\_c1}\right|\left|a_1\right|\left|S_{32\_c1}\right|\left|a_2\right|\cos\left(\phi_{1\_c1} - \phi_{2\_c1} + \varphi\right)\end{pmatrix} \quad (5)$$

$$P_{sum\_c2} = \frac{1}{2}\cdot\left(\left|b_{sum\_c2}\right|^2\right) = \frac{1}{2}\cdot\left(\left|S_{31\_c2}a_1 + S_{32\_c2}a_2\right|^2\right)$$
$$= \frac{1}{2}\cdot\begin{pmatrix}\left|S_{31\_c2}\right|^2\left|a_1\right|^2 + \left|S_{32\_c2}\right|^2\left|a_2\right|^2 + \\ 2\left|S_{31\_c2}\right|\left|a_1\right|\left|S_{32\_c2}\right|\left|a_2\right|\cos\left(\phi_{1\_c2} - \phi_{2\_c2} + \varphi\right)\end{pmatrix} \quad (6)$$

where S_{31}, S_{32}, are the measured 3-port system S-parameters if the shortest phase-shift cable is used in the reference probe signal path. The three ports of the SA system are illustrated in Fig. 1. S_{31_c1}, S_{32_c1} are the measured 3-port system S-parameters if the phase-shift cable 1 is used in the reference probe signal path, and S_{31_c2}, S_{31_c2} are the measured 3-port system S-parameters if the longest phase-shift cable 2 is used in the reference probe signal path. $\emptyset_1$ is the phase of S_{31}, and $\emptyset_2$ is the phase of S_{32}. Similarly, the other $\emptyset$ are the phase of the corresponding S-parameters while using phase-shift cable 1 and phase-shift cable 2. The input parameters in (4-6) are $|a_1|$, $|a_2|$, and φ. Where, $|a_1|$ is the input signal from the reference probe at a fixed location to the reference probe signal path. Similarly, $|a_2|$ is the input signal from the scanning probe over the DUT scan plane to the main probe signal path.

The measured values of P_{sum}, P_{sum_c1}, and P_{sum_c2} are row matrices of [6 x 1] dimension, obtained from the three phase-shift cables. Here, the six values represent the six different control voltages which lead to a step size of approximately 5 dB in the voltage controlled attenuator. This attenuation is introduced on the reference probe signal path prior to the summation at the combiner component. The scanning sequence for the automated single frequency and broadband frequency measurement scenarios are explained in detail.

- In general, there are three steps required during the phase measurement using the SA method. In the first scanning step, the main probe signal path amplifier is turned off, and the scanning probe is positioned away from the DUT. The net effect of these steps adds large attenuation on the main probe signal path. Thus, when the summation is measured at the SA, effectively the SA measures only the power from the reference probe signal path (P_{ref}). For instance, in (4), the contribution of a_2 is negligible due to the added attenuation on the main probe signal path. For the P_{ref} measurement, only one measurement is required.
- The second step requires the user to measure the probe powers (P_{main_probe}) from the DUT scan plane. For instance, if there are 100 points to be scanned over a DUT surface, then 100 measurements of the main probe signal power are performed over the DUT scan plane. To effectively measure only the main probe signal, attenuation is introduced on the reference probe signal path, by turning off the power supply for the amplifier and introducing maximum attenuation on the variable attenuator in the reference path. As a consequence, in (4), the contribution of a_1 is negligible due to the added attenuation on the reference probe signal path.
- The third step involves measuring the summation of the main probe signal path and the reference probe signal path. Here, depending on the single or multiple frequency measurement scenario, the number of summation measurements need to determined. For instance, for a single frequency operation, after the reference probe path (P_{ref}) and the main probe (P_{main_probe}) magnitudes are measured, the two magnitudes can be compared, and the attenuation level can be identified at which the two signals have similar magnitudes. After identifying the attenuation level, the voltage controlled attenuator is set at the required attenuation, and the summation of the reference probe signal and the main probe signal is measured. Here, only three measurements (one for each phase-shift cable) are needed for the third scanning step.
- However, in a broadband measurement scenario where multiple frequencies are of interest, and one does not know a priori which frequencies shall be analyzed, one needs to capture data at different attenuator levels such that for one of the data sets each signal will have an amplitude that is comparable to the amplitude of the reference signals. At this point, there are a few possible algorithmic choices to proceed with the measurement. First, measure the reference and the main probe signal spectrum. Then, identify the frequencies of interest. Second, measure the magnitude for both the reference probe and the main probe signals at each of the multiple frequencies of interest. Third, identify the attenuation value on the variable attenuator at which the two inputs have similar magnitudes for each frequency of interest. Finally, only obtain the summation of the two input signals at the desired attenuation setting. Here, a total of three (one attenuation level and three phase-shift cables) measurements are needed. One limitation of this implementation is that the identification of the required attenuation to be added at each signal frequency of interest has to be done at each scan point, as the main probe signal magnitude will vary along the scan area. In addition, multiple signal frequencies will have different magnitudes, thus, requiring a different attenuation levels to be added and then obtain the summation measurements at a scan point. Hence, increasing the overall time required for near-field scanning.
- One solution to optimizing the scanning method is to perform the measurement 18 times at each scan point (six attenuation levels for each of the three phase-shift cables). If there are mulitple frequencies to be scanned, the optimization for scan time is possible, by performing the summation measurements at six attenuation levels for each phase-shift cable and postpone the correct attenuation setting identification to the post-processing step after the scan. In most real-world measurement scenarios, the multiple frequencies of interest will not have the same signal magnitude. Hence, the measurement with multiple attenuation levels are first obtained, and then the phase difference is calculated at multiple frequencies of interest based on the correct attenuation setting in post-processing steps. Fig. 3 depicts the flowchart, which illustrates the steps performed to determine phase in a broadband scan.
- To determine the phase difference $\varphi = \emptyset_{a2} - \emptyset_{a1}$, a fminsearch function in Matlab [19] which uses the Nelder-Mead simplex algorithm [20] is used to solve for the two unknowns which are the phase values of the reference and the main probe signal $\emptyset_{a1}$, and $\emptyset_{a2}$. First, different initial phase values are assigned to each of the two input signals $\emptyset_{a1}$, and $\emptyset_{a2}$. The two input signals $|a_1|$, $|a_2|$, and the system path S-parameters are known. Using the assigned phase values to the two inputs $|a_1|$ and $|a_2|$, analytically the summation terms are calculated. Then, the fminsearch algorithm iteratively minimizes the error between the SA measured powers and the analytically calculated powers. Fig. 3 depicts the flowchart, which illustrates the steps performed to determine phase in a

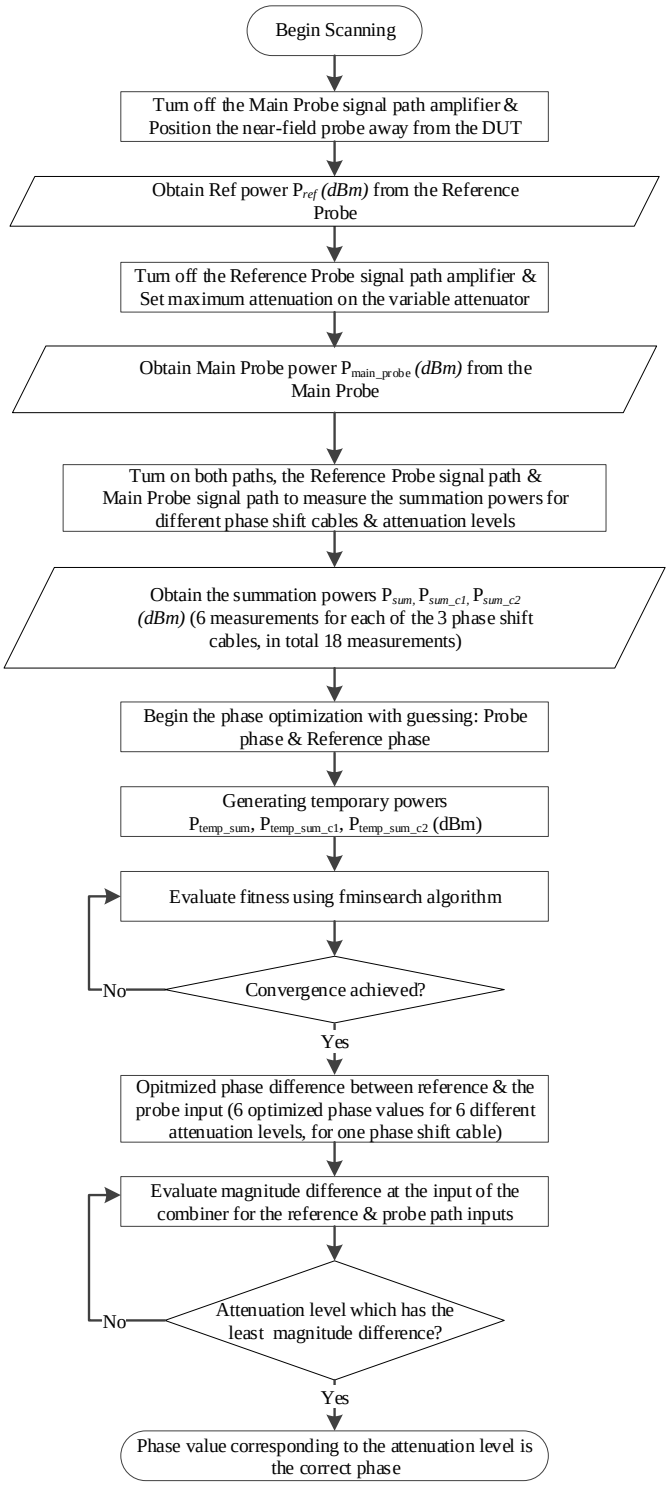

Fig. 3. SA based phase measurement flowchart for a broadband frequency scan.

broadband scan. The calculated powers are obtained using the following relations and are identified by adding temp subscript to the measured power variables names.

$$P_{temp\_sum} = \frac{1}{2}\cdot\left(\left|b_{temp\_sum}\right|^2\right) = \frac{1}{2}\cdot\left(\left|S_{31}a_{1\_start} + S_{32}a_{2\_start}\right|^2\right) \quad (7)$$

$$P_{temp\_sum\_c1} = \frac{1}{2}\cdot\left(\left|b_{temp\_sum\_c1}\right|^2\right) = \frac{1}{2}\cdot\left(\left|S_{31\_c1}a_{1\_start} + S_{32\_c1}a_{2\_start}\right|^2\right) \quad (8)$$

$$P_{temp\_sum\_c2} = \frac{1}{2}\cdot\left(\left|b_{temp\_sum\_c2}\right|^2\right) = \frac{1}{2}\cdot\left(\left|S_{31\_c2}a_{1\_start} + S_{32\_c2}a_{2\_start}\right|^2\right) \quad (9)$$

where $a_{1\_start} = |a_1|e^{j\emptyset a1\_start}$ and $a_{2\_start} = |a_2|e^{j\emptyset a2\_start}$

- The convergence of the optimization function is determined by the error function, whose value is minimized iteratively. The error function is defined by

$$Error = \left|P_{sum} - P_{temp\_sum}\right| + \left|P_{sum\_c1} - P_{temp\_sum\_c1}\right| + \left|P_{sum\_c2} - P_{temp\_sum\_c2}\right| \quad (10)$$

- A potential optimization problem lies in reaching the local minima during the iterative process. The problem can be avoided by testing different starting values and accepting the converged result as the best estimate. In this paper, the fminsearch function termination tolerance "TolFun" and "Tolx" were set to a value of 1e-30. However, these parameters can be further refined to reduce the computational time required to resolve the phase information.

B. VNA-Based Method

Fig. 4 depicts the setup used for near-field scanning measurements using API SmartScan phase measurement (PHM) scanning system [21]. The VNA [22] is set in tuned receiver mode for measuring the phase and magnitude information from the DUT. In this mode, the internal source power is deactivated. Thus, the VNA behaves like a dual-channel spectrum analyzer, but it can also measure the phase between the two channels. Since most of the available VNAs are not as good as an SA receiver in tuned receiver mode, due to poor image and spurious rejection limitations, the VNA is set to measure a single frequency in a zero span mode. A common setting of 200 KHz resolution bandwidth is selected for the SA, VNA, and oscilloscope instrument based measurement setups.

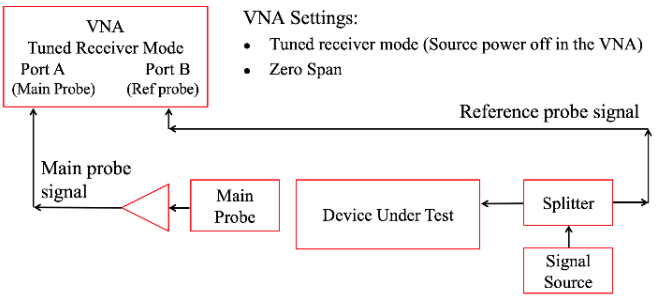

Fig. 4. VNA measurement setup block diagram.

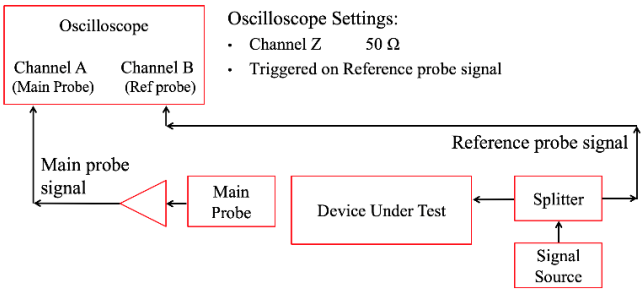

Fig. 5. Oscilloscope measurement setup block diagram.

C. Oscilloscope-Based Method

Fig. 5 depicts the setup used for near-field scanning measurements performed in time-domain using API SmartScan phase measurement (PHM) scanning system [21]. The oscilloscope [23] is triggered on the reference probe signal, which is assumed to be stable during the near-field scan. The time-domain data is transferred to the controlling computer, and the FFT is performed in Matlab [19]. Acquiring the time-domain data and then performing post-processing in Matlab provides flexibility in the settings used for FFT such as window functions etc. The oscilloscope measures the V_{peak} (peak voltage) of the time-domain signal. The V_{peak} is converted to V_{RMS} (root mean square voltage). A flat top window function is applied to the acquired time-domain data, and then FFT is performed to obtain the frequency-domain data. The frequency-domain resolution bandwidth is inversely proportional to the time-domain record length. The sampling rate and the number of points are determined to obtain a resolution bandwidth of the 200 KHz on the FFT data. The sampling rate of 20 GSa/s is chosen to be more than twice the desired 5 GHz signal frequency of interest.

IV. Measurement And Simulation Results

The three instrument-based methods are compared by performing near-field scanning over the same DUT as illustrated in Fig. 6. In addition, CST full-wave simulation [24] is used as a reference to compare against the three measurement methods. Fig. 7 depicts the DUT (a resonant structure at 5 GHz) over which the scanning was performed using a precise positioning robotic system. A 0.5 mm x 0.5 mm loop H-field probe was used to scan at an electric loop height of 0.4 mm above the DUT surface. Before initiating the scan, API H-field probe was evaluated over a calibration air trace structure [25] for its ability to reject or suppress the unwanted field components at 5 GHz. It is important to test the rejection ratio of the probe [10], as it defines if the probe can measure the desired E- or H-field component. Fig. 8 illustrates that the H-field probe used has about 8.5 dB suppression of the unwanted field components. Thus, making it suitable to be utilized for the near-field scanning application.

A. Measurements on the Resonant Trace Structure

The DUT scan area of 20 mm x 10.5 mm was scanned with a spatial resolution of 0.5 mm (about 900 scan points). The scan area is depicted in Fig. 7. The measured H_y component magnitude and the phase obtained using SA, VNA, and oscilloscope based methods are illustrated in Fig. 6. It should be noted that the phase difference obtained using the SA method is calibrated to a known trace structure at 5 GHz. In addition, all the cables, amplifiers, and adapter used during the measurement need to be calibrated out during the post-processing steps for the SA, VNA, and the oscilloscope methods. Any inaccuracies in the phase estimation of these components will introduce phase errors.

B. Full-Wave Simulation

The DUT geometry is imported to the CST MWS software. The simulated near-field data is obtained using the FIT time-

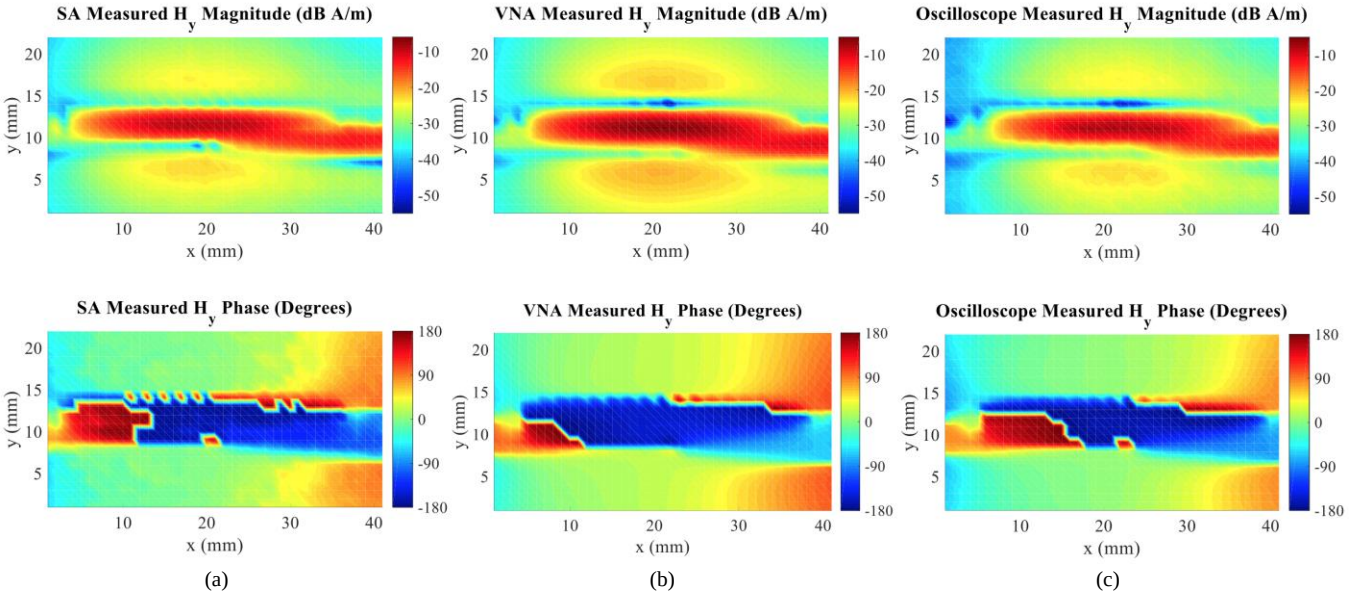

Fig. 6. Measured magnitude and phase of the H_y component at 5 GHz, 0.4 mm above the DUT surface. (a) Using the proposed spectrum analyzer method. (b) Using the VNA method. (c) Using the oscilloscope method.

domain solver at 0.4 mm above the DUT surface, where 0.4 mm height is equivalent to the electric loop height of the probe. A comparison of the S_{21} data of the measured and the simulated DUT trace is shown in Fig. 9 (b). The simulated H_y component magnitude and phase plots are illustrated in Fig. 10.

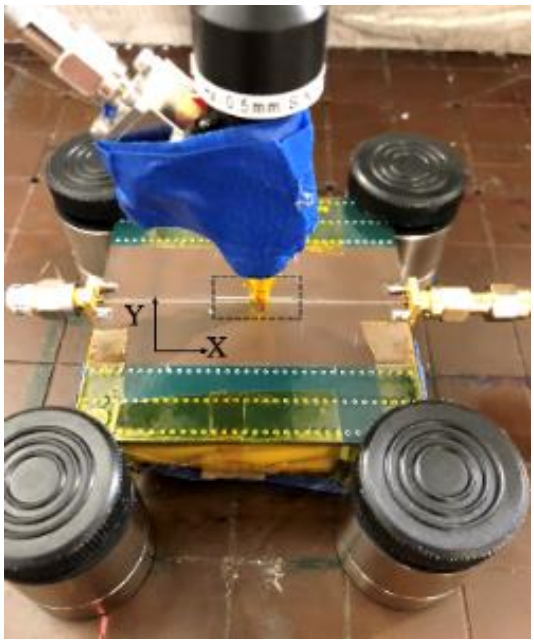

Fig. 7. Near-field scan over the resonant trace structure (DUT) using API's EMI probe Hx-0.5 [9] and SmartScan phase measurement (PHM) scanning system [21]. The dashed rectangle depicts the scan area over the DUT surface.

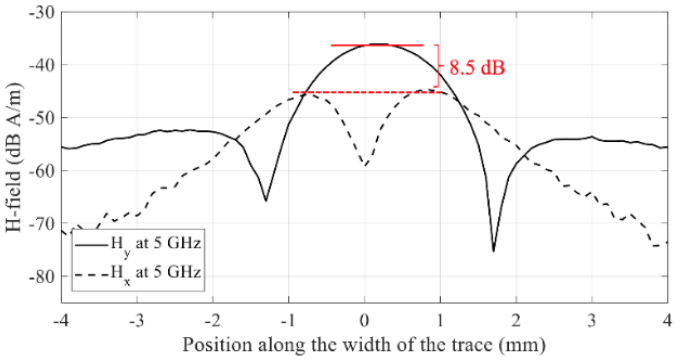

Fig. 8. H-field probe rejection ratio at 5 GHz measured at the height of 0.4 mm above the calibration trace. The H_y component is the desired component, and the H_x component is the undesired component of the calibration trace.

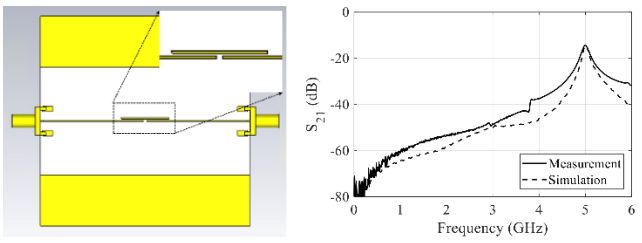

(a) (b)

Fig. 9. Full-wave simulation model (a) DUT is modeled in CST along with the SMA connectors. (b) The S_{21} comparison of the measurement and the simulated waveform. The simulated waveform shows a good agreement at the 5 GHz resonant frequency.

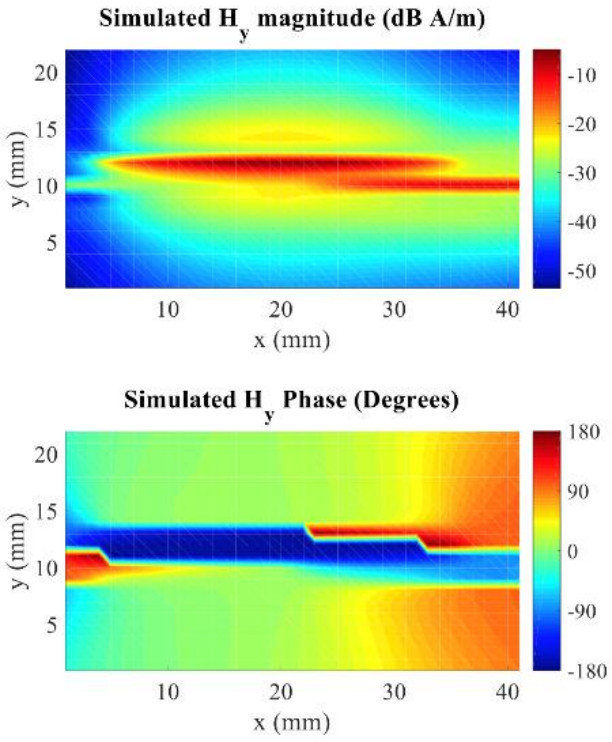

Fig. 10. Full-wave simulation (CST) model based magnitude and the phase distribution over the scan area as illustrated in Fig. 7.

C. *Comparison of the Different Methods*

The CST obtained data is compared with the three instrument based measurement methods of SA, VNA, and oscilloscope. Here, the simulated data is used as the reference data for performing the relative comparison. In order to quantify the difference in magnitude, the magnitude unit is converted from dB A/m to A/m units. The measurement method's magnitude is subtracted from the CST simulation obtained magnitude in linear scale units. The difference in magnitude for the three measurement methods to the simulation is presented in dB scale in Fig. 11. The measured phase is subtracted from the simulated phase. Any phase deviation observed in the delta values between the three relative error plots are introduced due to the measurement method.

V. Discussion

Fig. 11 illustrates the magnitude and phase differences between the simulation and the measurement methods. In the magnitude difference plots in Fig. 11, the strong regions are considered to be within 30 dB difference to the simulated fields. The weaker field regions shown in blue, relate to a difference in magnitude more than 30 dB to the simulated fields. The magnitude above the resonant trace structure (strong field region) has similar performance for the magnitude of the measured signal from the three measurement methods. However, the regions with more magnitude difference than 30 dB relate to weak field strength areas, which does not have much impact on the NFFFT or source reconstruction applications. Thus, the differences in magnitude in weak field regions can be neglected.

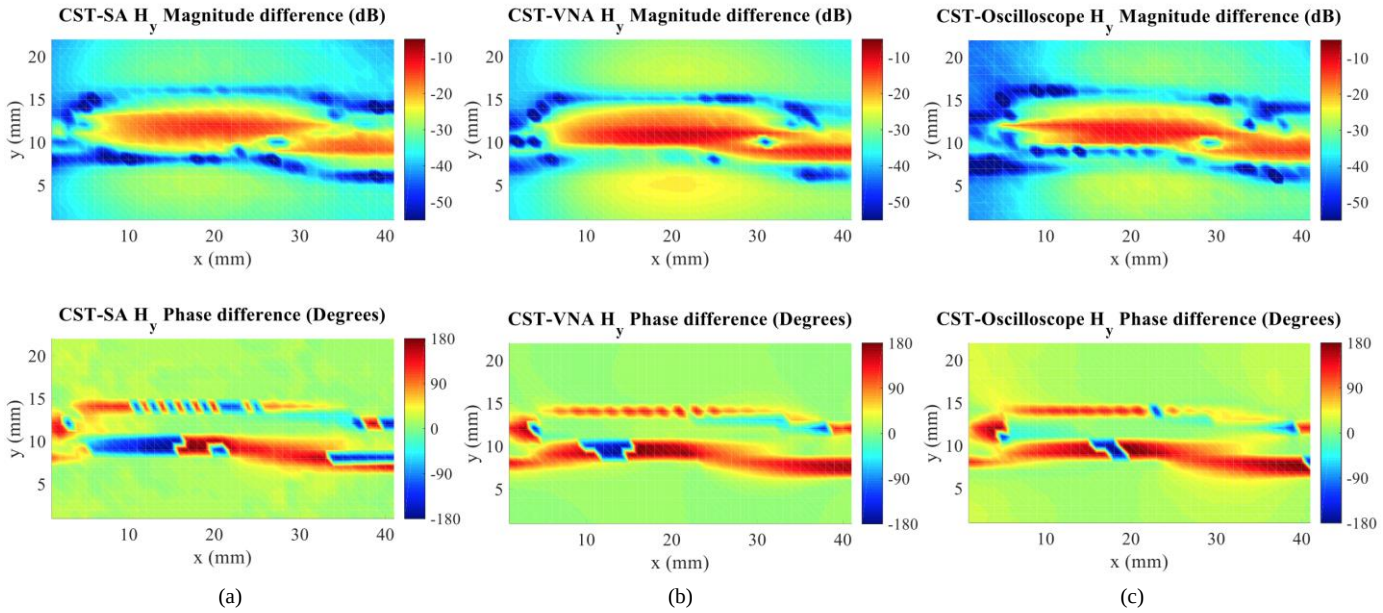

Fig. 11. Relative difference of the magnitude and the phase of the H_y component at 5 GHz, 0.4 mm above the DUT surface are illustrated. (a) Delta between the simulation and the SA measurement. (b) Delta between the simulation and the VNA measurement. (c) Delta between the simulation and the oscilloscope measurement.

Using CST simulation as a reference, the phase difference between the CST-VNA is about ± 10 degrees for the strong regions. Whereas, the phase difference between the CST-SA and the CST-Oscilloscope plots are about ± 20 degrees for the strong regions. This deviation is not considered to be critical [26], hence the performance of the SA and the oscilloscope is considered to be almost equal to performance of the VNA for single frequency scanning application. Table I discusses the relative advantages of a particular measurement instrument over the others based on the type of signals to be measured.

Other aspects, such as SNR, noise floor, dynamic range need to be considered during the measurements. One limitation arises from the implementation of the method, but it is not a principle limit of the methodology. The SA system shown in Fig. 1 has about a 35 dB system loss due to the use of the combiner, attenuators for reducing reflections, variable attenuators, etc., and introduces the requirement of minimum signal strength for this method. The SA using a 1 MHz RBW shows a noise floor of about -90 dBm (SA noise figure is about 20 dB). Thus, the reference and probe signals must have signal strengths >-55 dBm for achieving good phase resolution in the SA setup. If needed, further amplification could be added. Here, the best choice is a low noise amplifier directly at the probes [27].

If the measurement captures the phase of multiple signals, each having a different magnitude at once, the system needs to capture data at different attenuation levels. The reasons are that the best phase resolution is achieved if the reference probe signal and the main probe signal have approximately the same magnitude. The present implementation uses six steps of 5 dB each, leading to a 30 dB dynamic range between the stronger and the weakest signal that can be phase resolved. However, for

TABLE I
PHASE MEASUREMENT CONSIDERATIONS FOR DIFFERENT SIGNAL SPECTRUM SCENARIOS

MEASUREMENT SCENARIOS	SPECTRUM ANALYZER	VNA	OSCILLOSCOPE
Single frequency scan, with stable frequency	Slower than the VNA method. The frequency span setting on the SA will introduce longer sweep time, which may make SA slower than the oscilloscope method.	Fastest measurement method amongst the other methods as it has a fast sweep time and smaller file size.	Slower than the VNA method. The sampling rate and the time record will determine the file size, which can increase the time to scan leading to a comparable or longer time than the SA method.
Multiple frequencies	Faster than the VNA method, as it can measure multiple frequencies of interest and does not have the poor image and spurious rejection issue in a broadband measurement setting.	Needs multiple single frequency scans due to poor image and spurious rejection in a broadband measurement setting. Hence, a slower method.	Fastest measurement method to measure multiple frequencies in a wideband signal spectrum.
Multiple frequencies, scanning with lower RBW (<1 KHz)	The fastest measurement method amongst the other methods.	Needs multiple single frequency scans. Hence, a slower method.	Slow, as it takes long time due to long time record and large files sizes.
Transient event	Cannot capture, as the instrument measures in frequency-domain.	Cannot capture, as the instrument measures in frequency-domain.	Suitable method for measuring phase of transient signals.

a single frequency implementation, multiple attenuation measurements are not needed.

If a VNA is used, the ability to resolve the phase strongly depends on the signal present at the VNA. Most VNAs do not have image rejection, and they often show difficulty operating as tuned receivers if broadband noise and pulsing signals exist in addition to the signal that is desired. In addition, the VNA must be tuned to each frequency if multiple frequencies need to be measured. On the other hand, a VNA can only be effectively used on a single frequency scanning application at a time due to poor image and spurious rejection. First, an SA is required to identify the frequencies of interest from the DUT. Then, the scanning with VNA at zero span setting at the identified frequency is performed. If multiple frequencies are desired, then multiple scans at different frequencies are needed. Most VNAs can be set in spectrum analyzer mode; however, due to poor image and spurious rejection, they behave as poor spectrum analyzer receivers. However, a few high-end expensive VNAs provide the additional capability of spectrum analyzer mode [28] at an additional cost, where the VNA receiver works as a better spectrum analyzer.

An oscilloscope captures the time domain waveforms on multiple channels at the same moment. Applying a window function to the time-domain data is necessary before applying the FFT. The oscilloscope measures finite discrete time-domain data. If the number of periods in the time record is not an integer, the endpoints are discontinuous and a truncation error is introduced. These discontinuities show up as high-frequency components after the FFT. Thus, a smooth window function helps reduce the amplitude of the discontinuities at the ends of the acquired finite time record. There are different types of window functions such as uniform, hanning, hamming, Blackman-Harris, and flat top. Each type of window function has a different characteristic and application for the different types of signal spectrum. In this case, a flat top window is suitable for its amplitude accuracy in the frequency domain and a wider main lobe of the flat top window which allows measuring a stable phase value at the desired frequency of interest. Parameters which influence the ability to resolve phase are the record length, as it relates to the resolution bandwidth. Every oscilloscope has spurious signals, usually at multiples of the AD converter frequencies. The spurious free dynamic range is usually between 45-60 dB. If a spurious falls in the resolution bandwidth at the desired frequency, then the phase measurement may fail. On the other side, having four or more channels allows using multiple probes, and by using a trigger, a certain section of a time-varying waveform can be captured. Here, an example is the synchronization time frame in a video signal.

The comparison of the different instrument-based phase measurement methods in Table I illustrate that the VNA is a convenient method for a single frequency. For multiple frequency scanning, an oscilloscope is a better choice. However, because of the noisy signals spectrum, if a low RBW is desired, the SA method is a suitable choice. Based on different scanning signal properties such as the frequency stability, adjacent noise spectrum, transient events, a suitable instrument method needs to be determined by the EMC engineer for optimum phase measurement results.

VI. Conclusion

A broadband measurement method using a spectrum analyzer is proposed for phase-resolved near-field scanning. The method uses a set of external RF components such as phase shift cables, a variable attenuator, fixed attenuators, switches, and a combiner. The SA system bandwidth is determined by the frequency bandwidth of the individual external RF components used in the SA measurement. The method is capable of performing both single frequency, and broadband near-field scanning phase measurement. The SA-based phase measurement is performed over a resonant structure and compared with other known measurement methods using a VNA and an oscilloscope. In addition, the resonant structure was simulated in full-wave simulation software, and the simulated magnitude and phase were further compared with the measured SA, VNA, and oscilloscope methods.

References

[1] P. Maheshwari, H. Kajbaf, V. Khilkevich, and D. Pommerenke, "Emission Source Microscopy Technique for EMI Source Localization," *IEEE Trans. Electromagn. Compat.*, vol. 58, no. 3, pp. 729-737, Jun. 2016.

[2] C. A. Balanis, Advanced Engineering Electromagnetics. New York, NY, USA: Wiley, vol. 20, 1989.

[3] M. Sørensen, I. Bonev, O. Franek, G. Petersen, and H. Ebert, "How to handle a Huygens' box inside an enclosure," in Proc. IEEE Int. Symp. Electromagn. Compat., Aug. 2013, pp. 802–807.

[4] J. Pan, X. Gao, and J. Fan, "Far-Field Prediction by Only Magnetic Near Fields on a Simplified Huygens's Surface," *IEEE Trans. Electromagn. Compat.*, vol. 57, no. 4, pp. 693-701, Aug. 2015.

[5] H. Weng, D. G. Beetner, and R. E. DuBroff, "Prediction of radiated emissions using near field measurements," *IEEE Trans. Electromagn. Compat.*, vol. 53, no. 4, pp. 891–899, Nov. 2011.

[6] K. Kam, A. Radchenko, and D. Pommerenke, "On different methods to combine cable information into near-field data for far-field estimation," in Proc. IEEE Int. Symp. Electromagn. Compat., pp. 294-300, August 2012.

[7] G. Li, K. Itou, Y. Katou, N. Mukai, D. Pommerenke, and J. Fan, "A resonant E-field probe for RFI measurements," *IEEE Trans. Electromagn. Compat.*, vol. 56, no. 6, pp. 1719-1722, Dec. 2014.

[8] S. Shinde, S. Marathe, G. Li, R. Zoughi, and D. Pommerenke, "A Frequency Tunable High Sensitivity H-field Probe Using Varactor Diodes and Parasitic Inductance," *IEEE Trans. Electromagn. Compat.*, vol. 58, no. 1, pp. 331-334, Feb. 2016.

[9] EMI Probes. 2018. [Online]. Available: http://www.amberpi.com/products_EMI_probes.php

[10] S. Marathe *et al*., "Effect of Inhomogeneous Medium on Fields Above GCPW PCB for Near-Field Scanning Probe Calibration Application," *IEEE Trans. Electromagn. Compat.*, vol. 61, no. 1, pp. 3-10, Feb. 2019.

[11] "IEEE Standard for Calibration of Electromagnetic Field Sensors and Probes (Excluding Antennas) from 9 KHz to 40 GHz," IEEE Std 1309-2013 (Revision of IEEE Std 1309-2005), pp. 1–111, Nov 2013.

[12] J. Zhang, K. W. Kam, J. Min, V.V. Khilkevich, D. Pommerenke, and J. Fan, "An effective method of probe calibration in phase resolved Near-field scanning for EMI application," *IEEE Trans. Instrum. Meas.*, vol. 62, no. 3, pp. 648-658, Mar. 2013.

[13] T. Li, V. Khilkevich, and D. Pommerenke, "Phase-Resolved Near-Field Scan Over Random Fields," *IEEE Trans. Electromagn. Compat.*, vol. 58, no. 2, pp. 506-511, Apr. 2016.

[14] Y. Vives , C. Arcambal , A. Louis, F. de Daran, P. Eudeline, and B. Mazari, "Modeling magnetic radiations of electronic circuits using near-field scanning method," *IEEE Trans. Electromagn. Compat.*, vol. 49, no. 2, pp. 391-400, May 2007.

[15] Y. Vives-Gilabert, "Modelisation des emissions rayonnees des composants electroniques—Modeling magnetic emissions of electronic components," Ph.D. dissertation, Univ. Rouen, Rouen, France, 2007.
[16] Z.Chen, S. Marathe, H. Kajbaf, S. Frei, and D. Pommerenke, "Broadband Phase Resolving Spectrum Analyzer Measurement for EMI Scanning Applications," IEEE Int. Symp. Electromagn. Compat., pp. 1278-1283.
[17] S. Marathe, "Spectrum analyzer based phase measurement for EMI scanning applications," M.S. thesis, EMC Laboratory, Missouri S&T., Rolla, MO, USA, 2017.
[18] R&S FSVA/FSV Signal and Spectrum Analyzer Operating Manual. 2017. [Online]. Available: http://cdn.rohde-schwarz.com/pws/dl_downloads/dl_common_library/dl_brochures_and_datasheets/pdf_1/FSV_FL_dat-sw_en_3606-7982-22_v1001~1.pdf
[19] MathWorks MATLAB. 2018. [Online]. Available: http://www.mathworks.com
[20] J. C. Lagarias, J. A. Reeds, M. H. Wright, and P. E. Wright, "Convergence Properties of the Nelder-Mead Simplex Method in Low Dimensions," *SIAM Journal of Optimization*, vol. 9, no. 1, pp. 112–147, 1998.
[21] Phase Measurement scanning technology. 2018. [Online]. Available: http://www.amberpi.com/technologies_emission_phase_measurement.php
[22] Keysight 2-Port and 4-Port PNA-X Network Analyzer. 2017. [Online]. Available: https://literature.cdn.keysight.com/litweb/pdf/N5245-90008.pdf?id=1712187
[23] Keysight Technologies Infiniium 90000 Series Oscilloscopes. 2017. [Online]. Available: https://literature.cdn.keysight.com/litweb/pdf/5989-7819EN.pdf?id=1364807
[24] CST Microwave studio. 2016. [Online]. Available: https://www.cst.com/
[25] M. Sørensen, S. Marathe, D. Pommerenke, H. Kajbaf, and J. Min, "Design of TEM Transmission Line for Probe Calibration up to 40 GHz," in Proc. 2018 IEEE Int. Symp. Electromagn. Compat. Signal/Power Integrity, 2018, pp. 640–644.
[26] M. Sørensen *et. al.*, "Estimate on the uncertainty of predicting radiated emission from near-field scan caused by insufficient or inaccurate near-field data: Evaluation of the needed step size, phase accuracy and the need for all surfaces in the Huygens' box," in Proc. Int. Symp. Electromag. Compat., Rome, Italy, 2012, pp. 1–6.
[27] G. Maglakelidze, X. Yan, L. Guan, S. Marathe, Q. Huang, B. Bae, C. Hwang, V. Khilkevich, J. Fan, and D. Pommerenke "SNR Analysis and Optimization in Near-Field Scanning and EMI Applications," *IEEE Trans. Electromagn. Compat.*, vol. 60, no. 4, pp. 1087-1094, Feb. 2018.
[28] Keysight Technologies PNA and PNA-X Series Vector Network Analyzers Option 090 Spectrum Analyzer. 2015. [Online]. Available: https://literature.cdn.keysight.com/litweb/pdf/5992-0752EN.pdf

Shubhankar Marathe (S'14) received the B.E. degree in electronics and telecommunication from the University of Mumbai, Mumbai, Maharashtra, India in 2013, and the M.S. degree in electrical engineering from the Electromagnetic Compatibility (EMC) Laboratory, Missouri University of Science and Technology, Rolla, MO, USA, in 2017, where he is currently working toward the Ph.D. degree in electrical engineering at the EMC Laboratory.

In 2016, he was a Hardware Engineer Intern at Cisco Systems, RTP, NC, USA and in 2018, he worked as an EMC Design Engineering Intern at Apple Inc., Cupertino, CA. His research interests include Near-Field Scanning, Electrostatic Discharge, EMC Measurements and Signal Integrity.

Mr. Marathe was a recipient of the 2018 IEEE EMC Society President's Memorial Award at the Joint IEEE EMC & APEMC Symposium, Singapore, 2018.

Zongyi Chen received the M.S. degree in electrical engineering from China University of Mining and Technology, Xuzhou, Jiangsu, China in 2012. She was working as a Research Assistant at the On-Board Systems Lab, TU Dortmund University, Dortmund, Germany until the end of 2017. Currently, she is an Engineer at HELLA GmbH & Co. KGaA working on topics related to DC/DC converters.

Her research interests include EMC modeling of automotive electrical and electronic systems, Near-Field Scanning and Field-Prediction methods.

Kaustav Ghosh (S'16) received the B.E degree in electronics and telecommunication engineering from Nagpur University, India in 2012. He is currently working toward the M.S degree in electrical engineering from the Electromagnetic Compatibility (EMC) Laboratory, Missouri University of Science and Technology, Rolla, MO, USA.

His research interests include the numerical and experimental study of EMI problems at the system level and board level, analysis of EMI emission issues and different EMI mitigation approaches.

Hamed Kajbaf (S'08-M'12-SM'18) received the BS degree in electrical engineering from Shiraz University, Shiraz, Iran, in 2006 and he received the MS degree in biomedical engineering-bioelectric from Tarbiat Modares University, Tehran, Iran, in 2009. He received the PhD in electrical engineering from Missouri University of Science and Technology, Rolla, MO, in 2012.

He has previously worked at SpaceX as EMC Design Engineer. He is currently a Principal EMC Engineer at Amber Precision Instruments, San Jose, CA. His research interests include RF instrumentation, EMC and microwave scanning systems, near-field electromagnetic and acoustic measurement, and array signal acquisition/processing.

Stephan Frei (M'97-SM'13) received his Dipl.-Ing. degree in electrical engineering from Berlin University of Technology in 1995. Between 1995 and 1999 he was a research assistant for EMC at Berlin University of Technology, Institute of Electrical Power Engineering. From there he received his Ph.D. degree in 1999. Between 1999 and 2005 he worked at the automaker AUDI AG in the development department. Here he developed and introduced new methods for the computation of EMC, antennas and signal integrity in vehicles. Furthermore he was responsible for the EMC release process of several vehicles and international standardization. In 2006 he became a professor for vehicular electronics at TU Dortmund University, where his research interests are EMC, SI, computational methods, and vehicle power supply systems.

Dr. Frei is the author of more than 180 papers, and from 2008 to 2009 he served as Distinguished Lecturer for the IEEE EMC Society. Currently he is the Vice Dean of the Faculty for Electrical Engineering and Information Technology at TU Dortmund University.

Morten Sørensen (M'08) received the M.S. degree in physics from Aarhus University, Aarhus, Denmark, in 2005, and the Ph.D. degree in electrical engineering from Aalborg University, Aalborg, Denmark, in 2018. From 2006 to 2017, he was an antenna and EMC specialist with Bang & Olufsen, Struer, Denmark, including three years (2011-2014) as a researcher and technical project manager in the innovation consortium, EMC Design First Time Right. In 2017, he joined the EMC Laboratory, Missouri University of Science and Technology, Rolla, MO, USA, where he is a visiting assistant research professor. Since 2018 he has been working part time with Amber Precision Instruments, San Jose, CA, USA.

His current research interests include near-field scanning, emission source microscopy, electrostatic discharge, and system-level radiated emission.

David Pommerenke (F'15) received a Ph.D. degree from the Technical University of Berlin, Berlin, Germany, in 1996. After working with Hewlett Packard for five years, in 2001 he joined the EMC Laboratory, Missouri University of Science and Technology, Rolla, MO, USA, where he is currently a Professor. His current research interests include System-Level ESD, Electronics, Numerical Simulations, EMC Measurement Methods, and Instrumentation.

Dr. Pommerenke is an Associated Editor for the IEEE TRANSACTION ON ELECTROMAGNETIC COMPATIBILITY. He has authored or coauthored more than 200 papers, co-owner of a start-up company on EMC scanning and is the inventor on 13 patents.

Jin Min (Kyungjin) received the Ph.D. degree from the North Carolina State University, in 1998. After working at LSI Logic and Perkin Elmer for four years, he co-founded Global Technology Leader in 2004, and co-founded Amber Precision Instruments in 2006, where he is responsible for operations and technology development. His interests are development of EMC scan technologies and EMC scanners.

He has authored and co-authored more than 20 publications and holds six patents. He was a member of ESDA (Electrostatic Discharge Association) Standard Committee, involving component ESD and LU test standard revision and JEDEC and ESDA joint standard preparation.